3D dynamics of debris flows quantified at sub-second intervals from laser profiles

Mylène Jacquemart, Lorenz Meier, Christoph Graf & Felix Morsdorf

Natural Hazards
Journal of the International Society for the Prevention and Mitigation of Natural Hazards

ISSN 0921-030X

Nat Hazards
DOI 10.1007/s11069-017-2993-1

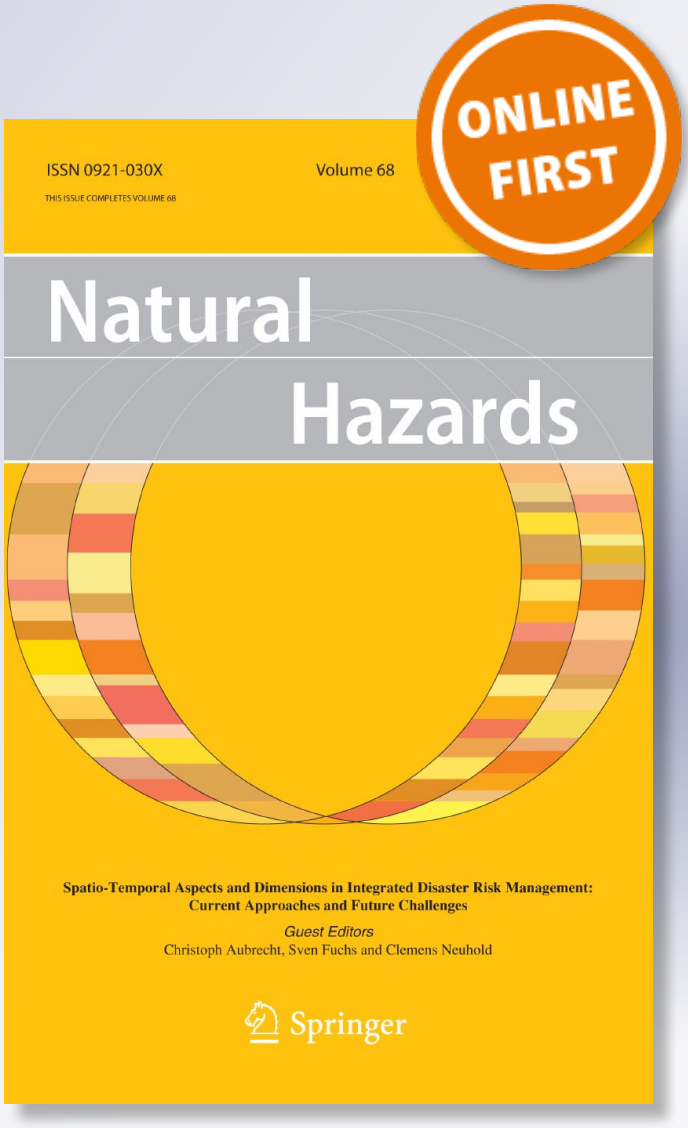

Springer

Nat Hazards
DOI 10.1007/s11069-017-2993-1

ORIGINAL PAPER

3D dynamics of debris flows quantified at sub-second intervals from laser profiles

Mylène Jacquemart[1,2,3] · Lorenz Meier[4] · Christoph Graf[2] · Felix Morsdorf[3]

Received: 27 January 2017 / Accepted: 12 July 2017

Abstract We use pairs of parallel mounted laser profile scanners to measure main debris-flow variables in two debris-flow channels in central and southern Switzerland. The scanners measure the instantaneous cross-sectional geometry of debris flows at rates of 25–100 Hz, and we apply large-scale particle image velocimetery to estimate velocity. The scanners also provide direct measurements of flow depth. From these data, we were able to estimate debris-flow depth, velocity and discharge for 16 out of 17 events. These results are consistent with discharge estimated from a system of geophones and a radar gauge for two available datasets. We also investigated debris-flow geometry to quantify rheology-controlled cross-flow convexity and found that four events manifest strong surface convexity at their surge fronts where we expect the largest boulders and low pore-fluid pressures. The scanners provide a completely new view of debris-flow dynamics and channel morphology and present novel opportunities to measure discharge and investigate debris-flow geometries.

✉ Mylène Jacquemart
mylene.jacquemart@colorado.edu

Lorenz Meier
lorenz.meier@geopraevent.ch

Christoph Graf
christoph.graf@wsl.ch

Felix Morsdorf
felix.morsdorf@geo.uzh.ch

[1] Present Address: CIRES, University of Colorado at Boulder, Boulder, CO, USA

[2] Swiss Federal Institute for Forest, Snow and Landscape Research WSL, Birmensdorf, Switzerland

[3] Remote Sensing Laboratories (RSL), University of Zurich, Zurich, Switzerland

[4] Geopraevent AG, Zurich, Switzerland

Published online: 02 August 2017

Keywords Debris flow · Laser scanning · LSPIV · Monitoring · Discharge · Rheology

1 Introduction

In this article, we report the successful measurement of debris-flow characteristics during their dynamic downhill translation phase. We quantify the flow height and discharge of several debris flows from repeat laser profiles acquired by two laser profile scanners suspended above the channels. In addition, we investigate the characteristic convex cross-flow geometries of flows in motion with the aim to relate these to debris-flow rheology.

Debris flows are gravity-induced mass movements common to mountainous regions around the world, and they cause severe damage to infrastructure and livelihoods every year (e.g., Hungr et al. 2001). They are distinguished by very rapid flow (0.5–20 ms^{-1}), variable water content and grain sizes ranging from clay to large boulders, typically showing some amount of rough sorting (Takahashi 2014; Hungr et al. 2001; Costa 1984).

As sediment availability in alpine regions is assumed to increase with rising temperatures (Gruber and Haeberli 2009), changes to snowmelt and precipitation patterns have the potential to alter the frequency and magnitude of debris flows in ever more densely populated alpine valleys (Huggel et al. 2012). Mitigation measures can only be reliable through a profound understanding of debris-flow translation dynamics (Graf et al. 2013; Tobler et al. 2014). Insights from numerical modeling have become increasingly important for engineering protection measures and for creating hazard maps (Rickenmann et al. 2006), and dynamic observational data that constrain these models are currently sparse (Hungr 2000).

With regard to hazard mitigation, Hungr (2000) emphasizes the importance of peak discharge, peak velocities and flow height as the main controls on debris-flow momentum, impact force, runout distance and ability to overrun channel walls and barriers. Modern debris-flow monitoring systems can provide measurements of these variables, and a wide variety of instruments have been used to achieve this (an overview is presented in, Arattano and Marchi 2008). Many systems rely on two types of sensors: Geophones can be placed along the channel side to measure the seismic signals of passing debris-flow surges or large boulders and used to compute the flow velocity. Ultrasonic, laser and radar gauges provide flow height information or, when used in pairs, can also provide the velocity component.

In the first part of this study, we present an ancillary approach relying on particle image velocimetry (PIV), an image analysis technique that can be used to compute displacement vectors from repeat temporal observations of visual features in order to derive flow velocities. Originating in laboratory environments (e.g., Rubino and Brandt 2003), PIV approaches have more recently been successfully applied to larger-scale problems and are thus often referred to as large-scale particle image velocity (LSPIV) (Fujita et al. 1998; Muste et al. 2008).

LSPIV offers distinct advantages over other gauging techniques because it does not require sensors to be in contact with the flow, and has proven suitable for measuring flow velocities during periods of high flow (Le Coz et al. 2010) by tracking natural features such as the surface patterns of turbulent water or floating debris (Dobson et al. 2014). Terrestrial laser scanners (TLS), on the other hand, provide unique tools to map our environment and measure changes within (Vosselman and Maas 2010). While TLS offer precise and high-resolution 3D information in static environments, they are not suited for dynamic processes, as the minimum duration of a 3D scan is on the order of several minutes. Line scanners, on the other hand, only provide a beam deflection on one axis (as opposed to two

for TLS) and can thus provide these high line-scan repetition rates, making them suitable for observing dynamic events. A number of teams have used repeat TLS point clouds to investigate the displacement fields of slower processes like landslides and rock glaciers in this manner (e.g., Kenner et al. 2014; Travelletti et al. 2014). To our knowledge, however, LSPIV methodology has never been applied to laser scanner data acquired over a rapidly evolving target such as a debris flow. The only mention of a laser profile scanner being used for debris-flow monitoring was found in Osaka et al. (2013), where a single scanner was used to measure channel cross sections.

We dedicate the second part of this paper to describing a simple approach for quantifying the cross-flow convexity of debris flows. Debris flows tend to construct abrupt steep fronts populated by large boulders, followed by more liquid tails that host finer materials emplaced by fluid flow (Costa 1984; Iverson 1997, 2003). As opposed to their liquid tails, where particles are suspended in water, the geometry of their coarse-grained fronts is governed by grain-to-grain interaction. Measurements of pore-fluid pressures at debris-flow heads show that they are essentially dry, restraining the downslope movement of the water-saturated tail (Iverson 1997). That these coarse-grained fronts also develop convex cross-sectional profiles that rise above the point to which they would otherwise fill the channel, has only been superficially described (Colhoun 1966; Eisbacher and Clague 1984). It is, however, visible in model results (Pudasaini et al. 2005), but has hitherto escaped field quantification. We hypothesize that debris flows exhibit convex geometries at and near the flow front where pore-fluid pressure is low.

2 Methods

2.1 Study sites and data acquisition

For the present study, two laser profile scanners were mounted on a platform 1 m apart in the flow direction to each produce sets of repeat distance profiles of the debris-flow channel. These high-frequency down-facing scanners are installed at two established debris-flow monitoring sites in the Swiss Alps, at Dorfbach (canton of Valais) and Spreitgraben (canton of Bern), and provide globally unique datasets to study debris-flow dynamics. Between 2011 and 2015, 17 debris flows were recorded by the laser scanners (15 at Dorfbach and two at Spreitgraben). In both cases, the scanners are part of extensive debris-flow warning and monitoring systems (Graf et al. 2013; Jacquemart et al. 2015) and are mounted on platforms suspended above the channel (see Fig. 1b). In the following, we describe the setup at Dorfbach. A slightly different setup is found at Spreitgraben, where the distance to the channel bed is larger and scanner beam divergence is smaller (3.6 mrad). More information about the Spreitgraben setup can be found in Jacquemart et al. (2015) and Tobler et al. (2014). The SICK LMS 511 scanners used at Dorfbach have an scan angle range of 190°, have a beam divergence of 11.9 mrad and can be set to different scan rates (see Table 1). At the maximum scan rate, the scanners acquire 100 full profiles per second across 190°. The scanners operate in the near infrared (905 nm), and the laser pulses are deflected using a rotating mirror. Distances are computed within a polar coordinate system using time of flight measurements. When operated at 50 Hz and at a distance of 10 m above the channel bed, the angular resolution is about 0.33°. The laser footprint is 12 cm and increases in size as the laser is diverted to the side (see Table 1). In the described situation, the laser footprint doubles about 17 m off-nadir (20 m from the

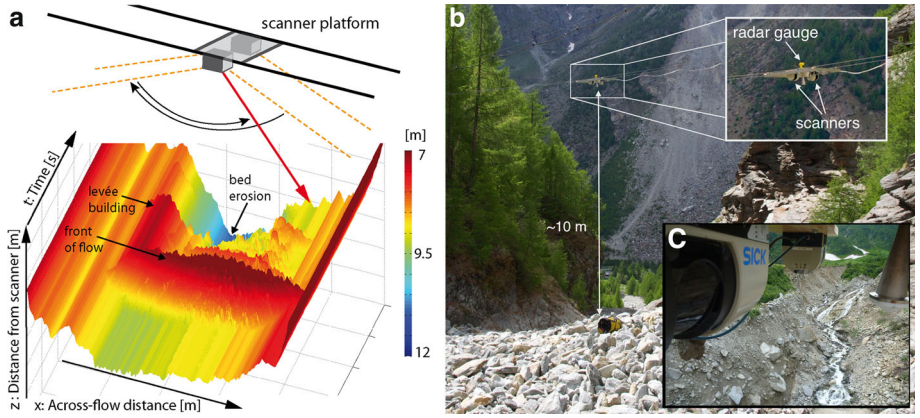

Fig. 1 **a** Visualization of 15,000 concatenated profiles with schematic scanner setup. Each data point is indexed with a coordinate *(x, t, z)*, where x = cross-flow distance, t = time and z = distance to scanner within a cartesian coordinate system. **b** Cables suspend a platform with two scanners and one radar gauge about 10 m above the channel at Dorfbach, and the scanners acquire single profiles at rates of up to 50 or 75 Hz. **c** Close up view of the scanners mounted below the platform at Spreitgraben

Table 1 The scanners angular resolution and point spacing on the ground depend on the scan rate

Scan rate settings			Geometric properties	
Scan rate [Hz]	Angular resolution [°]	Point spacing @ 10 m [m]	Distance to bed [m]	Resulting laser footprint [m]
25	0.167	0.0229	10	0.118
35	0.25	0.044	12	0.124
50[a]	0.5	0.087	14	0.166
75[b]	0.667	0.116	16	0.19
100	1	0.175	18	0.214

The footprint size depends solely on the distance to the bed

[a] Scan rate at Dorfbach after 2011

[b] Scan rate at Dorfbach in 2011 and Spreitgraben

scanner) if the channel bed was flat, but the concave geometry of the channel bed reduces this effect significantly. The point spacing in the raw data is listed in Table 1. When deployed, the actual point spacing and footprint depend strongly on the channel geometry and morphology. Geophones mounted on large boulders upriver of the gauging station start the scanners as soon as a passing debris flow is detected. All data are stored on a local PC from which it needs to be downloaded locally at regular intervals. In addition, the station is equipped with a camera and a radar gauge.

At Dorfbach, debris-flow velocities and discharge have historically been estimated by using the geophone signals to calculate the flow velocity and the radar gauge to measure flow height. Without the laser scanners, the geometry of the channel must be measured (or approximated) and it has been assumed that the flow fills the channel evenly. This approach has proven reliable in many cases (Badoux et al. 1008; Hürlimann et al. 2003;

Schlunegger et al. 2009). Arattano and Marchi (2005) have demonstrated that cross-correlation algorithms can help calculate flow velocities from geophone data or data from multiple radar or ultrasonic gauges even where no clear debris-flow front is present. Before the scanners were mounted, the estimation of flow velocity and discharge at Dorfbach has proven to be difficult because the wide channel allows the debris flows to move far away from the instruments, resulting in very poor quality of geophone data and sometimes missing the radar gauge entirely. The total costs for the two systems are very similar, but the laser scanners offer more flexibility and new views of debris-flow dynamics that have not been available to date (see Fig. 1).

2.2 Preprocessing

The files generated by the scanners contain time stamps, distance (r), angle (φ) and reflectance values. First, we transform the polar coordinates of the raw data (r, φ) to cartesian coordinates *(x, z)*, resulting in an irregular point cloud. We chose to identify each point P with a coordinate P *(x, z)* in the cartesian system because z denotes the height above the x-axis. We then interpolate all points to a regular grid with a 5-cm spacing in the cross-flow direction (x-axis). In most cases, it is necessary to limit the data in both space and time, because the scanners' field of view is wider than the bed and the recording extends past the time of a passing debris flow. The scanners record 50 single profiles per second, and the profiles can be concatenated to form 2.5-D image-like matrices, where x is the cross-flow distance in meters, t is the time in seconds and the matrix contains values of distance from the scanner (z), as is shown in Fig. 1a. Values below a certain user-defined threshold (we used 4 m distance from the scanner) are ignored in subsequent processing.

We have not experienced problems with rain during debris-flow events, but on September 1, 2015, a very liquid debris-flow at Spreitgraben caused dense mist, so that the scanners could not detect the surface of the flow. However, the raw data usually contain some undesired points in the air above the flow (possibly caused by rain in some cases) or very high peaks that might have been caused by splashing from the flow itself. To remove these points, we smooth the data by applying a 3×3 cell moving-window median filter. In order not to remove valuable surface roughness information, we plot the residuals between the original and smoothed data, removing only data points that exceed $3\ \sigma$ of the residual range. Comparisons of the filtered to the non-filtered surfaces showed that removing points exceeding $1\ \sigma$ or even $2\ \sigma$ remove too much surface information. All the remaining points are returned to the filtered signal unchanged.

2.3 Estimating flow height, velocity and discharge

2.3.1 Flow height computation

Knowledge of the channel bed geometry is a prerequisite for computing flow height that is difficult to quantify in a natural channel. Since it is impossible to know what happens to the alluvial bed during a debris flow, we decided to compute two bed geometries for each debris flow. We do this by averaging ten seconds worth of profiles from one scanner once before (t_1) and once after each debris flow (t_2). The bed geometry profiles ($z_0(t_i); i = 1, 2$) allow the flow height *(h)* at every point *(x, t)* to be calculated as:

$$h(x,t) = \begin{cases} 0, & \text{if } z(x,t) \leq z_0(x,t_i) \\ z(x,t) - z_0(x,t_i), & \text{if } z(x,t) > z_0(x,t_i) \end{cases} \quad (1)$$

Subsequently, we compute two flow height matrices, assuming that the bed remains unchanged during the entire duration of a flow. The two flow height matrices allow us to compute two different discharge estimates (see Fig. 4) for each debris flow. The two different hydrographs provide an estimate of the uncertainty introduced by the unstable channel bed.

2.3.2 *Flow velocity computation based on LSPIV*

In the standard LSPIV approach, velocity is computed as $v = l/\Delta t$, where l is the spatial displacement as measured by cross-correlation and Δt is the known temporal offset between the two photographs. In our case, velocity is computed as $v = l_d/\Delta t$, where l_d is the known spatial distance between the two scan lines and Δt is the temporal displacement as measured by cross-correlation. Since the measured displacement describes a temporal rather than a spatial offset, the image orthorectification process at the beginning of photograph-based LSPIV can be omitted.

Displacement computation is thence essentially identical to standard LSPIV as described in Dobson et al. (2014), Le Coz et al. (2010) or Aryal et al. (2012). The data matrix from the upstream scanner is divided into small subsets, or interrogation windows (IW), and appropriate parts of the data matrix from scanner 2 are searched for the best match (search windows; SW). The size of these windows has received significant attention in scientific literature. For classical PIV approaches, Raffel et al. (2007) state that the size of the SW must be at least three times larger than the maximum expected displacement within the IW, and Hu et al. (1998) emphasize that the IW must be smaller than the SW and at least twice the size of the maximum displacement so as not to violate the Nyquist theorem. Furthermore, Meunier and Leweke (2003) argue that the size of the IW must be large enough to contain a sufficient number of pixels with unique values to estimate a cross-correlation function, preferably showing more than 10 – 20 particles. In the laser datasets, the length (technically the *duration* l_t) of these windows is given by the expected flow velocities: For lower velocities, the data from the down-flow scanner need to be searched over a longer period of time, while for high velocities the lag (or "waiting time") to the start of the search window relative to that of the interrogation window needs to be kept short. The width [m] of the IW and SW is termed lateral resolution.

The expected maximum and minimum velocities, as well as the lateral resolution, must therefore be defined manually. It is assumed that the lateral resolution can be defined based on the expected maximum particle size (1 m was used in this study). Defining the maximum and minimum velocity is more critical, especially because velocity is one of the key parameters being calculated. We combined findings from a sensitivity analysis with expert opinions to find the range best suited for the channel at Dorfbach. Discharge results are largely insensitive to changes of the velocity parameters (within a realistic range), but a general knowledge of the expected velocities (i.e., from video images) is helpful to constrain these. For Dorfbach, we chose a maximum velocity of 20 ms^{-1} and a minimum velocity of 0.1 ms^{-1}. At Spreitgraben, we used 10 ms^{-1} as maximum velocity because 20 ms^{-1} yielded an unreasonably high peak discharge, and a sensitivity analysis is not possible with a single event. To allow for particles to move about freely, the SW used is three times wider than the IW. As is common, the cross-correlation coefficient is used as

similarity index to find the displacement between the IW and the SW (e.g., Dobson et al. 2014; Le Coz et al. 2010; Muste et al. 2008). To remove any height offset between the two scanners, the correlation analysis is performed on a high-pass filtered surface of the original data (similar as in Kenner et al. 2014).

A cross-correlation coefficient (C) is computed at every time step $l_t/4$. Since outside the travel path of the debris flow C should be very low because the scanner views remain different throughout, a normalized cross-correlation matrix (C_{norm}) is also computed for the whole image. This is done by retaining the maximum C for every window and normalizing these with the maximum C found across all windows. Windows with C_{norm} smaller than 0.1 are then excluded. Furthermore, since debris is (reasonably) assumed to move only downstream, only the lower half of the cross-correlation matrix is searched for peak correlation values, thus excluding peaks that correspond to particles arriving at the downstream scanner before arriving at the upstream scanner.

Finally, to reduce the number of false detections (e.g., when splashes in both the IW and the SW produce high correlation coefficients), a quality criterion was introduced: The peaks in the correlation coefficient matrix must be wide enough to have come from the debris surface. A C-peak is considered valid if 18 out of 25 cells in the 5×5 cell neighborhood of the peak exhibit a value of 0.7 of the maximum itself. If this criteria is not met, the corresponding velocity measurement is discarded. The parameters of this criterion were based on size considerations of the prevalent boulders (5 cells correspond to 25 cm). They were then adjusted based on the sensitivity analysis which showed that introducing this criterion eliminates velocity outliers that were found to all hit the defined maximum velocity.

2.3.3 *Hydrograph computation*

The dimensions of the resulting velocity matrix are given by the number of steps ($l_t/4$) computed along the time axis and the number of lateral resolution steps on the x-axis. The cross-correlation analysis typically provides velocity estimates over the coarse, blocky parts of the flow, leaving a velocity matrix with some fraction of empty cells. We build on the crude assumption that a higher flow height corresponds to a higher flow velocity, interpolating the unknown velocity (v_{int}) as

$$v_{\text{int}}(x,t) = \tilde{v}(t) \cdot \frac{h(x,t)}{h_{\max}(t)} \tag{2}$$

where $\tilde{v}(t)$ is the median velocity along each line t. If a line t has no velocity estimates from the cross-correlation, interpolation (Eq. 2) is not performed there.

This matrix is then upsampled to the resolution of the flow height matrix using nearest neighbor resampling. From there, computing the hydrograph is a straightforward sum of discharge per cell along every line t and total discharge is simply the cumulative sum of that over the entire duration of the debris flow. This is described in Eqs. 3 and 4, in which $\dot{Q}$ [m^3/s] is the discharge across every line t, X is the total number of cells in the cross-flow direction, h is in meters, L_c is the grid cell width [m], $v(x, t)$ is the corresponding flow velocity, Q is the total discharge in m^3, T is the total duration of the event in seconds and s is the sampling rate. For the final estimate, gaps originating from lines t without velocity estimates are filled by computing discharge values using the event-wide mean velocity.

$$\dot{Q} = \sum_{x=1}^{X} h(x,t) \cdot L_c \cdot v(x,t) \tag{3}$$

$$Q = \sum_{t=1}^{T} \dot{Q} \cdot \frac{1}{s} \tag{4}$$

A hydrograph was computed for each of the 14 debris flows at Dorfbach and for the 2014 event at Spreitgraben. Detailed results are presented in Sect. 3.

2.4 Curvature estimation

We parametrized the surface curvature normal to the flow direction by fitting and analyzing a fourth-order polynomial to every acquired laser profile. Similar approaches with second-order polynomials have been used by geomorphologists to describe glacial troughs (Hürlimann et al. 2003; Pattyn and van Huele 1998). While a second-order polynomial would be sufficient to describe the cross-sectional convex surface of the flow, it would require knowing the width of the flow which is a dynamically changing parameter. In a first step, we therefore apply a binary classification to distinguish profiles that exhibit some amount of curvature from those that do not. This can easily be distinguished from the number of zero crossings of each polynomial's first derivative. A profile is flagged as *convex* if its first derivative has three zero crossings or flagged as *not convex* in all other cases. If the debris-flow channel is empty, or filled with material that does not contribute to the described convex front, the approximated polynomial forms a parabolic trough (with only a single zero crossing). In addition, the first coefficient of the polynomial must be greater than zero in order to exclude polynomials that are up side down with respect to the expected channel geometry. Using the knowledge of which profiles exhibit the sought-after convexity, the amount of build-up the debris-flow front exhibits is expressed in two descriptive curvature factors computed as:

$$cf_W = \frac{h}{W} \tag{5}$$

and

$$cf_H = \frac{h}{H} \tag{6}$$

where h is the height of the local maximum above the average height of the two minima, W is the distance between the two minima and H is the maximum flow depth of the channel (see Fig. 2).

3 Results

3.1 Flow height, flow velocities and discharge

Of the 17 debris flows recorded between 2011 and 2015 at Dorfbach and Spreitgraben, we could evaluate all but one event (Spreitgraben, September 1, 2015, likely because spray and mist obscured laser returns). For the remaining 16 debris flows, we computed a pre-event and a post-event bed geometry in all but two cases, while velocity estimates were

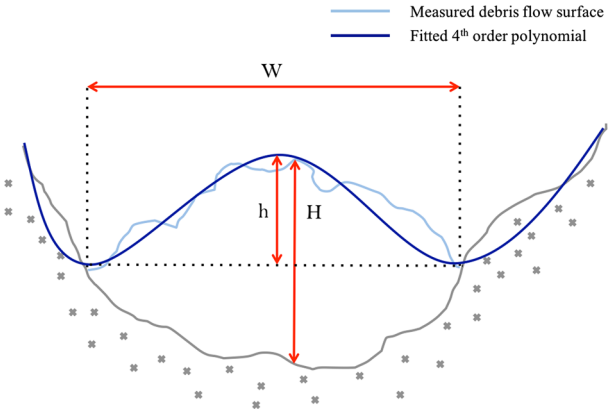

Fig. 2 Schematic cross section of a debris flow, showing the measured and fitted polynomial and the parameters chosen to describe surface convexity, flow thickness and width

always possible (see example in Fig. 3). Hydrographs were thus computed for 16 out of 17 events, while data derived from the radar gauge and geophones only allowed a discharge computation in two cases. In all other cases, the geophone data were not suitable to compute a flow velocity, making it impossible to generate a hydrograph. Table 2 shows the comparison of the laser-derived values to those estimated with geophones and the radar gauge, and Table 3 lists all values computed from the laser data for the remaining debris flows. For comparison, we have also included the flow height obtained from the radar gauge. We stress, however, that these measurement techniques are fundamentally different. The scanners measure the distance to individual points spaced only a few centimeters apart, with a footprint of about 10 cm, at very high temporal resolutions. The radar gauge

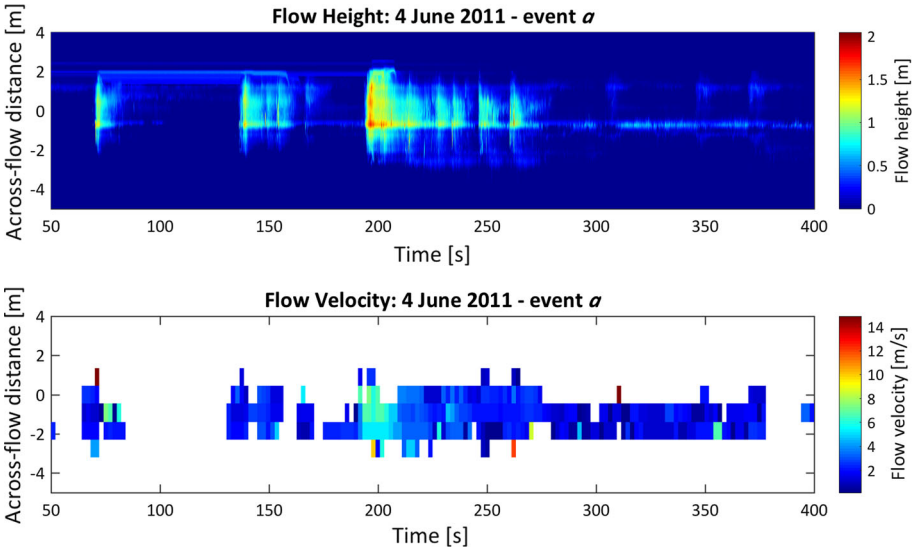

Fig. 3 Flow velocity and flow height fields used to generate the June 4, 2011 (event *a*), discharge (only the flow height generated with the post-flow geometry is shown in this example). The dimensions of the flow velocity cells depend on the chosen parameters (lateral resolution, expected minimum and maximum velocity), and this coarse velocity field is interpolated and upsampled before the hydrograph (Fig. 4) is generated

Table 2 Comparison of main debris-flow variables derived from repeat laser profiles and a combination of geophones and a radar gauge for the June 4, 2011, events. ± ranges indicate difference between runs with pre-event bed geometry and post-event bed geometries. For instance, for h_{max} 2 m ± 0.15 m, one run yielded 1.85 m and the other 2.15 m

Date	Q [m^3s^{-1}]	Q_{max} [m^3s^{-1}]	v_{max} [ms^{-1}]	v_{min} [ms^{-1}]	v_{mean} [ms^{-1}]	h_{max} [m]
Laser derived						
4.6.2011*a*	875 ± 85	29.5 ± 1.5	15	0.15	2.4	2.25 ± 0.15
4.6.2011*b*	975 ± 190	29 ± 5	15	0.2	2.5	2 ± 0.15

Date	Q [m^3s^{-1}]	Q_{max} [m^3s^{-1}]	v_{front} [ms^{-1}]	h_{max} [m]
Geophone/radar derived				
4.6.2011*a*	1125	18	4.1	0.9
4.6.2011*b*	700	11	2.4	0.5

Table 3 Main debris-flow variables measured for events at Dorfbach and Spreitgraben(*) between 2011 and 2014 from repeat laser profiles. Where more than one event per day was recorded they are labeled alphabetically. h_{max_L} denotes the maximum flow height derived from the laser scanners, h_{max_R} that from the radar gauge

Date [d.m.y]	Q [m^3]	Q_{max} [m^3s^{-1}]	v_{max} [ms^{-1}]	v_{min} [ms^{-1}]	v_{mean} [ms^{-1}]	h_{max_L} [m]	h_{max_R} [m]
3.6.2012*a*	80 ± 10	7.8 ± 0.1	13.32	0.13	1.4	1.6 ± 0.1	
3.6.2012*b*	550 ± 40	25.45 ± 0.65	9.92	1.28	3.5	2 ± 0.05	
3.6.2012*c*	880 ± 150	54 ± 0.25	13.23	0.13	2.1	2.53 ± 0.03	
2.7.2012*a*	254 ± 45	9 ± 0.5	9.92	0.73	4.17	1.14 ± 0.04	
2.7.2012*b*	170 ± 100	6.2 ± 2.5	13.23	0.14	0.4	1 ± 0.2	
2.7.2012*c*	280 ± 0	19 ± 2	9.9	0.55	2.6	1.19 ± 0.04	0.73
2.7.2012*d*	1120 ± 310	35.5 ± 3.5	13.23	0.14	1.6	2.2 ± 0.5	0.59
18.6.2013	1660 ± 130	131 ± 3	16.13	0.26	1.2	3.15 ± 0.03	2.8
6.6.2014	2115 ± 465	92 ± 20	10.75	0.22	3.1	2.5 ± 0.7	0.35
11.6.2014*a*	160	10.4	4.96	0.23	0.89	1.49	
11.6.2014*b*	3550	286.6	16.1	0.19	1.88	4.66	1.14
29.7.2014*a*	2305 ± 895	80.5 ± 14	16.2	0.14	2.14	2.3 ± 0.1	1.85
29.7.2014*b*	1315 ± 295	109.5 ± 7	12.9	0.11	1.4	4 ± 0.2	1.66
30.8.2014*	9975 ± 2515	197.5 ± 14.5	8.8	0.54	6.1	3.1 ± 0.4	
1.9.2015*	n.a.	n.a.	n.a.	n.a.	n.a.	n.a.	

integrates over a field of view of about 3 m once every second and is thus not able to capture individual peaks. Furthermore, the baseline for the flow height calculations from the laser scanners is an actual bed, whereas this is typically estimated from images or post-event field visits for the radar-derived flow height, and the geometry of the bed is

approximated to a trapezoidal shape. The hydrographs in Fig. 4 illustrate the variability in the resulting hydrographs depending on bed changes. The shaded range cannot be interpreted as a confidence interval, but illustrates how changes in the channel bed influence the discharge result.

3.2 Surface curvature

Four out of 16 events that the laser scanners could measure manifest clearly convex surfaces. The data in Fig. 5 are in stunning agreement with our hypothesis that convexity would be expected at the front of debris-flow surges where pore-fluid pressures are low and the coarse-grained fronts retain the fluid tail (Iverson 1997, 2003).

4 Discussion

We recognize that debris-flow discharge must be overestimated by the LSPIV approach, since we cannot resolve the vertical velocity decline. We considered applying a correction factor, but the validation data that we have do not provide a basis for this. More research and data will be needed to better understand this relationship. In the following sections, a more detailed discussion of the different processing steps is offered.

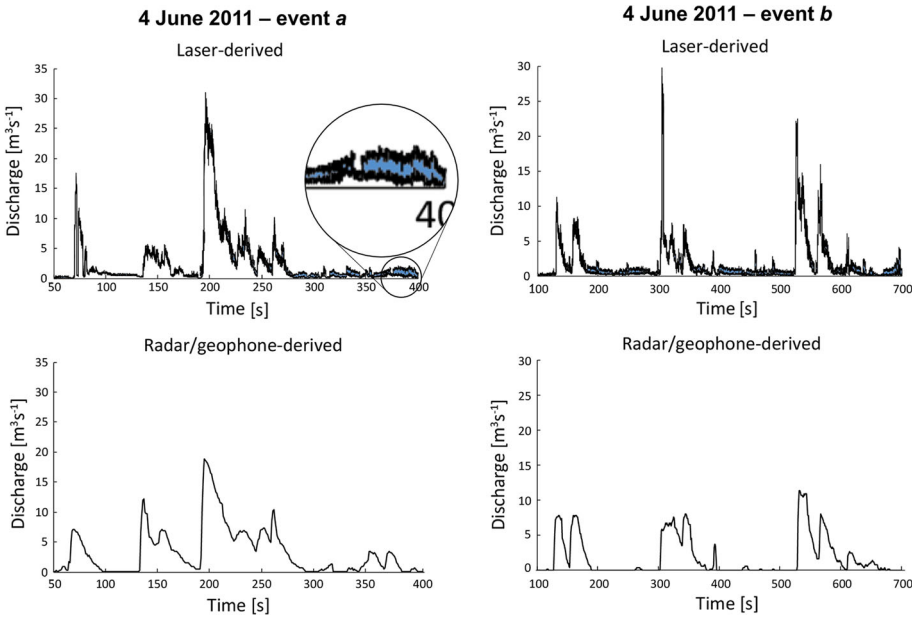

Fig. 4 Data from two debris flows recorded on June 4, 2011, at Dorfbach. The upper graphs show the laser-derived hydrographs, the lower feature hydrographs computed from the radar and geophone data. In the upper graphs, the *blue area* fills the range between the discharge calculated using the pre-event geometry and the post-event geometry. This difference is small in both these cases, but can be significant in others

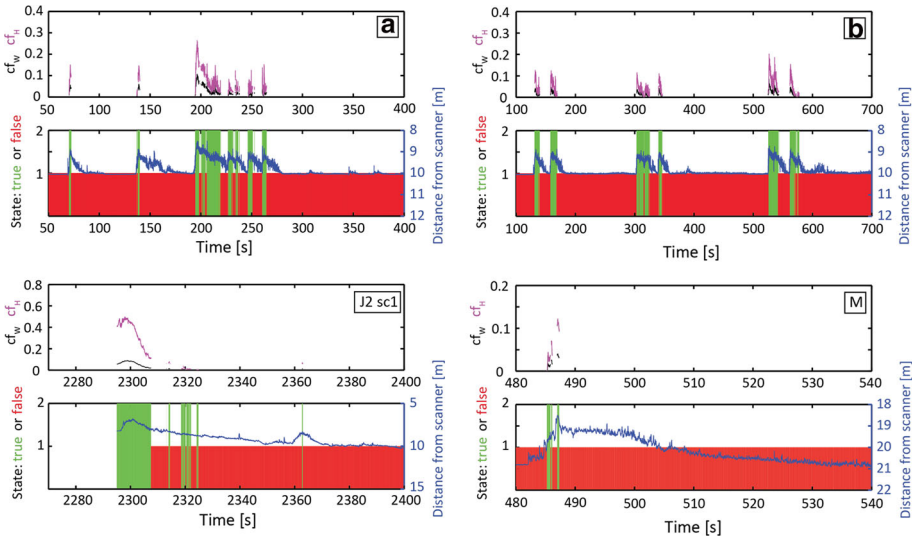

Fig. 5 Results from the curvature analysis. In the lower half of the plots, *green bars* indicate that surface convexity was detected for a given profile and *red bars* indicate the opposite. The *blue line* is an approximate center flow line that indicates when along the surge front surface convexity occurs. In the upper plots, the *magenta lines* represent curvature factors cf_H and *black lines* represent cf_w

4.1 Data processing

Most raw data errors can be eliminated by excluding points that are below the minimum threshold distance, the noise filtering and the averaging used to compute the bed geometry.

The fact that the scanners are suspended from cables above the channel makes them susceptible to wind-induced motion, but roll, pitch and yaw of the platform itself are not expected to dominate unless in severe storm. But it must be recognized that little movement is needed to disrupt the scan pattern, and lighter winds could cause vertical motion of the platform. We analyzed the amount of scatter found in distance measurements on the highest parts of the channel walls, i.e., the part of the bank that we assume to be stable. As such, we would expect the temporal changes in distances from the scanners, across all measurements, to be small. We calculated the mean standard deviation of distance to the scanners across all raw datasets on the stable banks to be 12 mm. Based on the field evidence from both sites, this is estimated to be at least one order of magnitude smaller than the surface roughness, and thus negligible. Another source of error are the parts of the channel that are hidden from the scanners, and where the missing values are automatically filled by linear interpolation when constructing the regular grid. This surface clearly does not represent the real surface of the debris flow. Working with data from terrestrial laser scanners, Aryal et al. (2012) show that interpolation over shadowed areas can create errors in the PIV solution, but the near-vertical view of the suspended scanners makes the holes in these datasets small, and we do not get PIV solutions for any of these regions. Therefore, the linear interpolation does not introduce any significant errors.

4.2 Debris-flow characteristics

Changes in the bed geometry during an event are the greatest source of uncertainty in the final discharge result. Debris flows are known to strongly erode their beds and entrain material, or they can deposit a part of their load, and both processes are possible during an event (Berger et al. 2010). Using a static bed for the entire duration of the debris flow is pragmatic, and this can only be partly improved by computing a second bed geometry following the event. It is, however, a simple and effective way of estimating the influence of bed changes on the discharge. Defining multiple points in time where a bed geometry is computed could improve this, but would come at higher computational costs, and the benefit of it should be investigated in detail. It must be stated, however, that this problem is inherent to any debris-flow discharge computation lacking a static bed (Hürlimann et al. 2003). Yet, in contrast to the established method of using radar or ultrasonic gauges, the laser profile scanners offer unprecedented accuracy for quantifying spatiotemporal changes in the channel bed below the scanner position. Additionally, if changes in flow path occur, the large coverage of the scanners provides a distinct advantage over radar or ultrasonic gauges that need to be centered over the flow.

A further issue is introduced by the flow height computation method (Eq. 1) that does not allow for negative flow height. Whenever a debris flow erodes its bed to a deeper stage than that prior to the event, all flow over that area is disregarded or underestimated. On the other hand, flow is generally overestimated where levées are deposited and misidentified as flow height and because no velocity decrease in the vertical flow profile is considered.

Applying LSPIV to concatenated laser profiles constitutes a novel approach to deriving surface flow velocities for debris flows, and the results are in good accordance with the values from the established system. The velocity computations are all within the expected range. Additionally, regions with cross-correlation values that are above the minimum cross-correlation threshold and that pass the quality criterion are persistently identified at the debris-flow fronts and slightly behind them, not during sequences where the channel is empty or water flow is expected. This indicates that the cross-correlation works in areas where the surface is in fact in motion and the roughness is high enough for a displacement to be identified. Within a reasonable range, results are robust to changes in processing parameters. Furthermore, comparison of the velocities recorded for individual events reveals a significant difference between the Spreitgraben and Dorfbach events. Such a difference would have been expected based on events previously observed at the two sites (Graf et al. 2013; Tobler et al. 2014).

The measured point velocities are applied to entire cells, whose size depends on the chosen parameters. Velocity outliers can therefore have a large influence on peak discharge. Although not applied to debris flows, Dobson et al. (2014) use a Gaussian interpolation considering neighboring values to compute a sub-pixel interpolation of the velocity matrix. Introducing such a smoothing step could significantly reduce the influence of isolated high velocity estimates and maybe provide more reliable peak discharge values.

In terms of recorded velocities, one event in 2014 (event 11.6.2014*a*) clearly stands out from the rest. This event was recorded on video and it was so slow that it stopped beneath the scanners, and a visualization shows a very clear structure of boulders at the surface. The following event (11.6.2014*b*) cleared the entire channel of debris almost instantly, presumably running into the debris deposited by event *a* at high speed. Comparing identical subsets of the two events' surfaces raises the question as to where the upper velocity

limit lies in the cross-correlation. As particles move faster, their representation gets compressed in the time dimension, complicating feature matching.

Generating a hydrograph from the flow height and flow velocity matrices is a technically straightforward task. One source of error introduced by the processing is the velocity interpolation. We recognize that using a linear interpolation does not capture the complex, nonlinear relationship between flow height and flow velocity (Iverson 1997; Prochaska et al. 2008; Rickenmann 1999). However, in the absence of any other known parameters describing flow characteristics, we believe that using the median (cross-flow) velocity for each line is a reasonable approximation, as it respects velocity gradients that have been observed throughout the duration of a debris-flow event (Arattano and Marchi 2000). The applied strategy can be problematic where flow is narrowly channelized and where the velocity interpolation is based on a very small number of observations. Additionally, where levée deposits are identified as flow height, a discharge value will be computed there as long as at least one velocity measurement exists along that profile.

We consider it likely that peak discharge is overestimated in many cases because the influence of the single velocity cells is large while the regions of peak flow height areas are usually small. However, the accuracy of the final discharge volume is primarily dependent on the magnitude of the changes to the bed geometry. The shaded range between the two estimates plotted in Fig. 4 emphasizes this. The comparison of values in Table 2 shows that the maximum flow height derived from the laser data is higher than that from the radar gauges, which can be expected based on the large footprint of the radar gauge. What is remarkable about the laser-based approach is that a discharge could be computed for every single event. This constitutes a significant improvement over traditional installations that rely on velocities computed from coarse and sometimes unreliable geophone readings.

4.3 Surface curvature

The surface convexity detection and parametrization presented in this study are the first of their kind. We hypothesized that the formation of a convex surface is an immediate consequence of the internal dynamics of the debris flow and its grain size distribution, or rheology (Costa 1984; Iverson 1997, 2003; Iverson et al. 2010). The major shortcoming in the current method is that only the polynomials are analyzed. In order to come to more reliable conclusions about the shape of the surface throughout a debris flow, the extrema identified on the polynomials could be used to find the corresponding maximum and minimum in the original data. Visual inspection of some of the polynomials suggests that the height of the maximum is often underestimated, while the minima are often overestimated. In some cases, when a convexity was readily identifiable to the unaided eye, the proposed algorithm nevertheless failed to identify the phenomenon. These errors were due to the geometric structure of the channel being complicated by deposited levées, so a more flexible approach is needed. The results suggest that curvature factors also depend on channel geometry, but the number of analyzed events is too small to come to more definite conclusions about this relationship. Alternatively, Hungr (2000) hypothesized that pronounced debris-flow heads take time to mature. This could explain why surface convexity was not found for all events.

The curvature factor cf_H suggests that up to 50% of the total flow thickness can come from the formation of the convex surface geometry. This is based on the assumption that the highest point on the curve overlies the deepest point in the channel, which is not necessarily true. However, these results indicate that post-event mudline observations in debris-flow channels may not always be reliable indicators of maximum flow height. The

fact that surface convexity is persistently detected at the surge heads suggests that the surface curvature can be used as a proxy for the longitudinal rheology, indicating the spatial separation between the coarse-grained front and the water-saturated tail of a debris flow.

5 Conclusion

We presented an novel approach that applies large-scale particle image velocimetry to concatenated laser profiles to compute the main debris-flow variables and investigate debris-flow geometry. Requiring minimal manual adjustment, this system successfully measured debris-flow discharge, velocity and flow height even in a location where the flow path within a channel is highly variable. Furthermore, it provides unprecedented temporal and spatial data describing debris flows and channel dynamics. The largest sources of uncertainty and error are assumptions concerning changes in shape of the channel bed during the debris flows and the use of surface velocity for discharge calculation. Our assessment of debris-flow surface geometries shows that debris flows can exhibit a clear cross-sectional surface convexity at and near the surge front, which we presume to be controlled by the ensemble dynamic rheology of the water-rock matrix.

Acknowledgements The authors are very grateful to Dr. Roger Bilham for all his valuable input and reviews and to Nate Stevens for proofreading the manuscript. We would also like to thank two anonymous reviewers for their contributions to improving this publication.

References

Arattano M, Marchi L (2000) Video-derived velocity distribution along a debris flow surge. Phys Chem Earth B Hydrol Oceans Atmos 25(9):781–784. doi:10.1016/S1464-1909(00)00101-5

Arattano M, Marchi L (2005) Measurements of debris flow velocity through cross-correlation of instrumentation data. Nat Hazards Earth Syst Sci 5(1):137–142

Arattano M, Marchi L (2008) Systems and sensors for debris-flow monitoring and warning. Sensors 8:2436–2452

Aryal A, Brooks BA, Reid ME, Bawden GW, Pawlak GR (2012) Displacement fields from point cloud data: application of particle imaging velocimetry to landslide geodesy. J Geophys Res 117:1–15. doi:10.1029/2011JF002161

Badoux A, Graf C, Rhyner J, Kuntner R, McArdell BW (1008) A debris-flow alarm system for the Alpine Illgraben catchment: design and performance. Nat Hazards 49:517–539

Berger C, McArdell BW, Fritschi B, Schlunegger F (2010) A novel method for measuring the timing of bed erosion during debris flows and floods. Water Resour Res. doi:10.1029/2009WR007993

Colhoun EA (1966) The debris-flow at Glendalough, Co. Wicklow and the bog-flow at Slieve Rushen, Co. Cavan January 1965. Ir Nat J 15(7):199–206

Costa JE (1984) Physical geomorphology of debris flows. In: Fleisher PJ, Costa JE (eds) Developments and applications of geomorphology. chap 9. Springer, Berlin, pp 268–317

Dobson DW, Holland KT, Calantoni J (2014) Fast, large-scale, particle image velocimetry-based estimations of river surface velocity. Comput Geosci 70:35–43. doi:10.1016/j.cageo.2014.05.007

Eisbacher GH, Clague JJ (1984) Destructive mass movements in high mountains: hazard and management. Minister of Supply and Services, Ottawa

Fujita I, Muste M, Kruger A (1998) Large-scale particle image velocimetry for flow analysis in hydraulic engineering applications. J Hydraul Res 36(3):397–414. doi:10.1080/00221689809498626

Graf C, Deubelbeiss Y, Bühler Y, Meier L, McArdell BW, Christen M, Bartelt P (2013) Gefahrenkartierung Mattertal: Grundlagenbeschaffung und numerische Modellierung von Murgängen. In: Graf C (ed) Mattertal—ein Tal in Bewegung, Publikation zur Jahrestagung der Schweizerischen Geomorphologischen Gesellschaft, St. Niklaus, Switzerland, 29, pp 85–112

Gruber S, Haeberli W (2009) Mountain permafrost. In: Margesin R (ed) Permafrost soils, Springer. Bio Ser, vol 16, pp 33–44
Hu H, Saga T, Kobayashi T, Okamoto K, Taniguchi N (1998) Evaluation of the cross correlation method by using PIV standard images. J Vis. 1(1):87–94
Huggel C, Clague JJ, Korup O (2012) Is climate change responsible for changing landslide activity in high mountains? Earth Surf Process Landf 37(1):77–91. doi:10.1002/esp.2223
Hungr O (2000) Analysis of debris flow surges using the theory of uniformly progressive flow. Earth Surf Process Landf 25:483–495
Hungr O, Evans SG, Bovis MJ, Hutchinson JN (2001) A review of classification of landslides of the flow type. Environ Eng Geosci 7(3):221–238
Hürlimann M, Rickenmann D, Graf C (2003) Field and monitoring data of debris-flow events in the Swiss Alps. Can Geotech J 40:161–175
Iverson R (1997) The physics of debris flows. Rev Geophys 35(3):245–296
Iverson R (2003) The debris-flow rheology myth. In: Rickenmann D, Chen CL (eds) 3rd International conference on debris-flow hazards mitigation: mechanics, prediction and assessment, 1, pp 303–314
Iverson RM, Logan M, LaHusen RG, Berti M (2010) The perfect debris flow? Aggregated results from 28 large-scale experiments. J Geophys Res 115(F3):F03,005. doi:10.1029/2009JF001514
Jacquemart M, Tobler D, Graf C, Meier L (2015) Advanced debris-flow monitoring and warning system at Spreitgraben. In: Lollino G, Arattano M, Rinaldi M, Giustolisi O, Marechal JC, Grand GE (eds) Engineering geology for society and territory, vol 3. Springer, Cham, pp 59–62
Kenner R, Bühler Y, Delaloye R, Ginzler C, Phillips M (2014) Monitoring of high alpine mass movements combining laser scanning with digital airborne photogrammetry. Geomorphology 206:492–504. doi:10.1016/j.geomorph.2013.10.020
Le Coz J, Hauet A, Pierrefeu G, Dramais G, Camenen B (2010) Performance of image-based velocimetry (LSPIV) applied to flash-flood discharge measurements in Mediterranean rivers. J Hydrol 394(1–2):42–52. doi:10.1016/j.jhydrol.2010.05.049
Meunier P, Leweke T (2003) Analysis and treatment of errors due to high velocity gradients in particle image velocimetry. Exp Fluids 35(5):408–421. doi:10.1007/s00348-003-0673-2
Muste M, Fujita I, Hauet A (2008) Large-scale particle image velocimetry for measurements in riverine environments. Water Resour Res. doi:10.1029/2008WR006950
Osaka T, Takahashi E, Kunitomi M, Yamakoschi T, Nowa Y, Kisa H, Ishizuka T, Utsunomiya R, Yokoyama K, Mizuyama T (2013) Field observations of unit weight of flowing debris flows by force plate in Sakurajima, Japan. J Jpn Soc Eros Control Eng 65(6):46–50
Pattyn F, van Huele W (1998) Power law or power flaw? Earth Surf Process Landf 23:761–767
Prochaska AB, Santi PM, Higgins JD, Cannon SH (2008) A study of methods to estimate debris flow velocity. Landslides 5(4):431–444. doi:10.1007/s10346-008-0137-0
Pudasaini SP, Wang Y, Hutter K (2005) Modelling debris flows down general channels. Nat Hazards Earth Syst Sci 5(6):799–819. doi:10.5194/nhess-5-799-2005
Raffel M, Willert CE, Wereley ST, Kompenhans J (2007) Particle image velocimetry, a practical guide. Oxford University Press, New York
Rickenmann D (1999) Empirical relationships for debris flows. Nat Hazards 19(1):47–77
Rickenmann D, Laigle D, McArdell BW, Hübl J (2006) Comparison of 2D debris-flow simulation models with field events. Comput Geosci 10(2):241–264. doi:10.1007/s10596-005-9021-3
Rubino A, Brandt P (2003) Warm-core eddies studied by laboratory experiments and numerical modeling. J Phys Oceanogr 33(2):431–435
Schlunegger F, Badoux A, McArdell BW, Gwerder C, Schnydrig D, Rieke-Zapp D, Molnar P (2009) Limits of sediment transfer in an alpine debris-flow catchment, Illgraben, Switzerland. Quartenary Sci Rev 28:1097–1105
Takahashi T (2014) Debris flow—mechanics, prediction and countermeasures, 2nd edn. CRC Press Taylor and Francis Group, London
Tobler D, Kull I, Jacquemart M, Haehlen N (2014) Hazard management in a debris flow affected area: case study from Spreitgraben, Switzerland. In: Sassa K, Canuti P, Yin Y (eds) Landslide science for a safer geoenvironment. Springer, Cham, pp 25–30. doi:10.1007/978-3-319-04996-0
Travelletti J, Malet JP, Delacourt C (2014) Image-based correlation of laser scanning point cloud time series for landslide monitoring. Int J Appl Earth Obs Geoinf 32:1–18. doi:10.1016/j.jag.2014.03.022
Vosselman G, Maas HG (eds) (2010) Airborne and terrestrial laser scanning. Whittles Publishing, Dunbeath